═══REVIEW COMMONS MANUSCRIPT═══

IMPORTANT:

- Manuscripts submitted to Review Commons are peer reviewed in a journal-agnostic way.
- Upon transfer of the peer reviewed preprint to a journal, the referee reports will be available in full to the handling editor.
- The identity of the referees will NOT be communicated to the authors unless the reviewers choose to sign their report.
- The identity of the referee will be confidentially disclosed to any affiliate journals to which the manuscript is transferred.

GUIDELINES:

- For reviewers: https://www.reviewcommons.org/reviewers
- For authors: https://www.reviewcommons.org/authors

CONTACT:

The Review Commons office can be contacted directly at: office@reviewcommons.org

Contraction-induced endocardial *id2b* plays a dual role in regulating myocardial contractility and valve formation

Shuo Chen[1, 2, 3], Jie Yin[1, 2, 3], Jinxiu Liang[1, 2, 3], Weijia Zhang[1, 2, 3], Peijun Jiang[1, 2, 3], Wenyuan Wang[4, 5], Xiaoying Chen[6, 7], Yuanhong Zhou[8], Peng Xia[8], Fan Yang[6, 7], Ying Gu[1,2, 3], Ruilin Zhang[4, 5], Peidong Han[1, 2, 3*]

[1]*Center for Genetic Medicine, The Fourth Affiliated Hospital, Zhejiang University School of Medicine, Hangzhou, Zhejiang, China.*

[2]*Institute of Genetics, Zhejiang University International School of Medicine, Hangzhou, Zhejiang, China.*

[3]*Division of Medical Genetics and Genomics, The Children's Hospital, Zhejiang University School of Medicine, National Clinical Research Center for Child Health, Hangzhou, Zhejiang 310058, China.*

[4]*TaiKang Medical School (School of Basic Medical Sciences), Wuhan University, Wuhan, China*

[5]*Hubei Provincial Key Laboratory of Developmentally Originated Disease, Wuhan, China*

[6]*Department of Biophysics, and Kidney Disease Center of the First Affiliated Hospital, Zhejiang University School of Medicine, Hangzhou, China.*

[7]*Liangzhu Laboratory, Zhejiang University Medical Center, Hangzhou, China.*

[8]*Zhejiang Provincial Key Laboratory for Cancer Molecular Cell Biology, Life Sciences Institute, Zhejiang University, Hangzhou, Zhejiang 310058, China.*

*To whom correspondence should be addressed.

hanpd@zju.edu.cn

+86-571-88206360

Abstract

Biomechanical cues play an essential role in sculpting organ formation. Comprehending how cardiac cells perceive and respond to biomechanical forces is a biological process with significant medical implications that remains poorly understood. Here we show that biomechanical forces activate endocardial *id2b* (inhibitor of DNA binding 2b) expression, thereby promoting cardiac contractility and valve formation. Taking advantage of the unique strengths of zebrafish, particularly the viability of embryos lacking heartbeats, we systematically compared the transcriptomes of hearts with impaired contractility to those of control hearts. This comparison identified *id2b* as a gene sensitive to blood flow. By generating a knockin reporter line, our results unveiled the presence of *id2b* in the endocardium, and its expression is sensitive to both pharmacological and genetic perturbations of contraction. Furthermore, *id2b* loss-of-function resulted in progressive heart malformation and early lethality. Combining RNA-seq analysis, electrophysiology, calcium imaging, and echocardiography, we discovered profound impairment in atrioventricular (AV) valve formation and defective excitation-contraction coupling in *id2b* mutants. Mechanistically, deletion of *id2b* reduced AV endocardial cell proliferation and led to a progressive increase in retrograde blood flow. In the myocardium, *id2b* directly interacted with the bHLH component *tcf3b* (transcription factor 3b) to restrict its activity. Inactivating *id2b* unleashed its inhibition on *tcf3b*, resulted in enhanced repressor activity of *tcf3b*, which subsequently suppressed the expression of *nrg1* (neuregulin 1), an essential mitogen for heart development. Overall, our findings identify *id2b* as an endocardial cell-specific, biomechanical signaling-sensitive gene, which mediates intercellular communications between endocardium and myocardium to sculpt heart morphogenesis and function.

Keywords: Zebrafish, Heart, *id2b*, Valve, Contraction

Introduction

The heart develops with continuous contraction, and biomechanical cues play an essential role in cardiac morphogenesis[1,2]. Blood flow is directly sensed by the surrounding endocardium, which undergoes multiscale remodeling during zebrafish heart development. In the atrioventricular canal (AVC) endocardium, oscillatory flow promotes valvulogenesis through transient receptor potential (TRP) channel-mediated expression of Krüppel-like factor 2a (*klf2a*)[3-5]. Meanwhile, mechanical forces trigger ATP-dependent activation of purinergic receptors, inducing expression of nuclear factor of activated T cells 1 (*nfatc1*) and subsequent valve formation[6]. In the chamber endocardium, blood flow induces endocardial cells to adopt chamber- and region-specific cell morphology during cardiac ballooning[7]. A recent study further emphasizes that blood flow is essential for endocardial cell accrual in assembling the outflow tract[8]. Beyond their role in endocardial cells, proper biomechanical cues are indispensable for shaping the myocardium. For instance, in contraction compromised *tnnt2a*[9] and *myh6*[10] mutants, trabeculation is markedly reduced. Moreover, apart from the tissue-scale regulatory effect, the shape changes[11] and myofibril content[12] at the single-cardiomyocyte level are also sculpted by the interplay of contractility and blood flow in the developing heart.

In ventricular myocardium morphogenesis, biomechanical forces coordinate intra-organ communication between endocardial and myocardial cells by regulating BMP, Nrg/Erbb, and Notch signaling. The Nrg-Erbb axis stands as one of the most extensively studies signaling pathway mediating cell-cell communications in the heart[13-15]. In particular, endocardial Notch activity induced by cardiac contraction promotes the expression of Nrg, which then secretes into the extracellular space, binding to Erbb2/4 receptor tyrosine kinases on cardiomyocyte and promoting their delamination[16,17]. In agreement with the pivotal role of this signaling pathway in heart development, genetic mutations in zebrafish *nrg2a* and *erbb2* result in severely compromised trabeculae formation[18-20].

The development of cardiomyocytes encompasses the specification of subcellular structure, metabolic state, gene expression profile, and functionality[21,22]. The rhythmic contraction of cardiomyocytes relies on precisely regulated excitation-contraction coupling (E-C coupling), transducing electrical activity into contractile forces. This intricate signaling cascade involves membrane action potential, calcium signaling, and sarcomeric structure[23]. Specifically, membrane

depolarization triggers the opening of L-type calcium channel (LTCC), allowing calcium influx. The calcium signaling then activates the ryanodine receptor on the sarcoplasmic reticulum (SR) membrane, releasing additional calcium[23]. E-C coupling is essential for heart development, as evidenced by the complete silence of the ventricle and reduced cardiomyocyte number in *cacna1c* (LTCC α1 subunit in zebrafish) mutant[24]. Beyond its role in modulating cardiac structure formation, previous studies indicate that Nrg-Erbb2 signaling is also necessary for cardiac function, as *erbb2* mutants exhibit severely compromised fractional shortening and an immature conduction pattern[18,25]. However, the precise mechanism through which the blood flow-Nrg-Erbb2 axis controls cardiomyocyte functionality remains poorly understood.

Results

Transcriptome analysis identifies *id2b* as a blood flow sensitive gene

Blood circulation is dispensable for early embryonic development in zebrafish, presenting an ideal model to investigate biomechanical cues influencing heart morphogenesis. To identify genes affected by cardiac contraction or blood flow, we treated *myl7:mCherry* zebrafish embryos with tricaine to inhibit cardiac contractility from 72 hours post-fertilization (hpf) to 96 hpf. Hearts from control and tricaine-treated zebrafish embryos were manually collected under a fluorescence stereoscope as previously reported[26]. Subsequently, approximately 1,000 hearts from each group were subjected to RNA sequencing (Fig. 1a). A total of 4,530 genes with differential expression were identified, comprising 2,013 up-regulated and 2,517 down-regulated genes. With a specific focus on identifying key transcription factors (TFs) affected by perturbing biomechanical forces, differentially expressed genes (DEGs) encoding TFs were enriched into signaling pathways through KEGG analysis. Interestingly, our analysis identified several pathways known to be involved in heart development, including the transforming growth factor beta (TGFβ) signaling and Notch signaling pathways (Fig. 1b). In particular, the scaled expression levels of the top 6 DEGs ($|\log_2 FC| \geqslant 0.585$), exhibiting up- or down-regulation, were listed (Fig. 1c). Notably, as a component of the helix-loop-helix (HLH) family, *id2b* is the zebrafish homolog of the mammalian Id2 gene, functioning as a transcriptional repressor. Intriguingly, Id2 has been shown to regulate the formation of the murine AV valve, a process notably

influenced by alterations in blood flow directionality. Consequently, we interrogated the expression and function of *id2b* in developing embryos.

Through quantitative real-time PCR (qRT-PCR) analysis on purified embryonic hearts, we observed a ~50% reduction in *id2b* mRNA level following tricaine treatment from 72 to 96 hpf compared to the control (Fig. 1d). Furthermore, in situ hybridization was performed to visualize *id2b* expression under tricaine or 10 uM blebbistatin (an inhibitor of sarcomeric function and cardiac contractility) treatment from 48 to 72 or from 72 to 96 hpf. Consistently, our results showed a reduction in *id2b* signal in contraction-deficient hearts compared to the control (Fig. 1e). Similarly, injection of a previously characterized *tnnt2* morpholino at the 1-cell stage also led to compromised contraction and diminished expression of *id2b* (Fig. 1f). Taken together, these results indicate that biomechanical cues are essential for activating *id2b* in embryonic hearts.

Visualization of the spatiotemporal expression of *id2b* in developing embryos

Due to technical challenges in visualizing the cell-type-specific expression of *id2b* in the developing heart using whole-mount in situ hybridization, we employed an intron targeting-mediated approach[27] to generate a knockin *id2b:eGFP* line. This method allowed us to achieve specific labeling without perturbing the integrity and function of the endogenous gene[27] (Fig. 2a). Comparison of *id2b:eGFP* fluorescence with in situ hybridization at 24, 48, and 72 hpf revealed a substantial recapitulation of the eGFP signal with that of endogenous *id2b* expression. The fluorescence was notably enriched in the heart, brain, retina, and notochord (Fig. 2b), mirroring observations from a previously reported *id2b* transgenic line generated through BAC-mediated recombination[28].

To further elucidate the spatiotemporal expression of *id2b* in developing hearts, we crossed *id2b:eGFP* with *myl7:mCherry* or *kdrl:mCherry*, labelling cardiomyocytes or endocardial cells, respectively. Confocal images revealed minimal, if any, presence of *id2b:eGFP* in *myl7:mCherry*$^{+}$ cardiomyocytes (Fig. 2c). In sharp contrast, clear co-localization between *id2b:eGFP* and *kdrl:mCherry* was evident at 48, 72, and 96 hpf (Fig. 2d). Interestingly, there was an absence of *id2b:eGFP* signal in *kdrl:mCherry*$^{+}$ endothelial cells in trunk blood vessel and brain vasculature (Fig.

2e). In adult hearts, *id2b:eGFP* fluorescence was enriched in the chamber endocardium and the endothelium lining AVC, outflow tract (OFT), and bulbus arteriosus (Fig. 2f).

Cardiac contraction promotes endocardial *id2b* expression through primary cilia but not BMP

Taking advantage of live imaging on developing embryos, we explored the *in vivo* dynamics of *id2b* in response to biomechanical force at single-cell resolution. When embryos were treated with tricaine or blebbistatin, the intensity of *id2b:eGFP* in atrial and ventricular endocardium was significantly reduced (Fig. 3a, b). Similarly, injection of *tnnt2a* morpholino also markedly suppressed *id2b:eGFP* signal (Fig. 3a, b), in agreement with the results obtained from in situ hybridization. Strikingly, the reduction in fluorescence intensity was particularly pronounced in AVC endothelial cells (Fig. 3a, b, asterisks).

We then explored how cardiac contraction modulated *id2b* expression. Given that endocardial cells can sense blood flow through primary cilia[29,30], we used a characterized morpholino[29] to knockdown *ift88*, an intraflagellar transporter essential for primary cilia formation. Previously work demonstrated a complete loss of primary cilia in endocardial cells upon *ift88* knockdown[29]. As expected, a significant decrease in *id2b:eGFP* intensity was observed in the chamber and AVC endocardium of *ift88* morphants compared to control (Fig. 3c, d), suggesting that biomechanical forces promote the expression of *id2b* via primary cilia. In the developing heart, a central hub for mediating biomechanical cues is the Klf2 gene, which includes the *klf2a* and *klf2b* paralogues in zebrafish[3-5,29,31]. Previous studies in mammals and zebrafish have highlighted the essential role of Klf2 transcription factor activity in cardiac valve and myocardial wall formation[3,31]. As a flow-responsive gene, *klf2a* expression has been observed throughout the entire endocardium, evidenced by mRNA expression and transgenic studies[3,4]. Interestingly, in situ hybridization on 48 and 72 hpf *klf2a*$^{-/-}$ and *klf2b*$^{-/-}$ embryos unveiled a drastic decrease in *id2b* expression compared with wild-type zebrafish (Fig. 3e), supporting the notion that *klf2*-mediated biomechanical signaling is essential for activating *id2b* expression.

Because *id2b* has been reported to be a target gene of bone morphogenetic protein (BMP) signaling, we explored whether BMP also played a role in regulating *id2b* when blood flow was perturbed. To this end, we knocked down *bmp2b*, *bmp4*, and *bmp7a* in 1-cell stage *id2b:eGFP* embryos and found a significant reduction in fluorescence signal in morpholino-injected hearts compared to

control (Supplementary Fig. S1a, b), suggesting that *id2b* is a target gene of BMP signaling during early embryonic development. Considering that heartbeats in zebrafish commence at approximately 22 hpf, we treated embryos with the BMP inhibitor Dorsomorphin from 24 to 48 hpf or from 36 to 60 hpf. While the number of endocardial cells was slightly reduced upon Dorsomorphin exposure, as previously reported[7], surprisingly, quantification of the average *id2b:eGFP* fluorescence intensity in individual endocardial cells revealed no significant differences between Dorsomorphin and DMSO controls (Supplementary Fig. S1c, d).

We further visualized BMP activity using the *Bre:dGFP* reporter line. Confocal images revealed strong fluorescence in the myocardium at 72 hpf, with minimal signal present in the endocardium except for the AVC endothelium (Supplementary Fig. S1e). Moreover, after tricaine treatment, endocardial *Bre:dGFP* slightly increased (Supplementary Fig. S1e), as opposed to the reduced *id2b:eGFP* signal (Fig. 3a, b). Likewise, endocardial *Bre:dGFP* intensity was barely affected after completely blocking contraction with *tnnt2a* MO injection (Supplementary Fig. S1e). These observations align with previous work using pSmad-1/5/8 as a readout of BMP activity, indicating that endocardial BMP signaling is independent of blood flow[7]. Collectively, these results suggest that BMP signaling and blood flow modulate *id2b* expression in a developmental-stage-dependent manner.

Compromised AV valve formation in *id2b* mutants

To investigate the role of the contractility-*id2b* axis in zebrafish heart development, we generated a loss-of-function mutant line using CRISPR/Cas9. A pair of sgRNAs designed to target exon 1 was injected with zCas9 protein into 1-cell-stage embryos. Consequently, we identified a mutant allele with a 157 bp truncation, leading to the generation of a premature stop codon (Fig. 4a). The overall morphology of *id2b* mutants (*id2b*$^{-/-}$) remained unaltered compared to *id2b*$^{+/+}$ siblings at 72 and 96 hpf (Fig. 4b). However, *id2b*$^{-/-}$ zebrafish were subjected to early lethality starting around 31 weeks post-fertilization (Fig. 4c). Strikingly, pericardial edema was observed in 20% (9/45) of adult *id2b*$^{-/-}$ zebrafish (Fig. 4d, top). Upon dissecting hearts from these *id2b*$^{-/-}$ zebrafish, a prominent enlargement in the atrium was detected (Fig. 4d, bottom). Histological analysis further revealed malformation in the AV valves of these *id2b*$^{-/-}$ mutants compared to the control (Fig. 4e). Upon closer inspection of AV

valve anatomy, we noted that the superior and inferior leaflets were significantly thinner, comprising only 1-2 layer of cells in *id2b*$^{-/-}$ zebrafish with an enlarged atrium. This was in sharp contrast to *id2b*$^{+/+}$ zebrafish, which exhibited multilayers of cells (Fig. 4e). Subsequent examination of the remaining 80% of *id2b*$^{-/-}$ zebrafish (36/45) that did not display prominent pericardial edema also revealed an enlarged atrium and AV valve malformation, albeit to a lesser extent (data not shown). In contrast, *id2b*$^{+/+}$ controls (48/48) displayed normal heart morphology with intact AV valve (Fig. 4e, left).

To further interrogate the effect of *id2b* inactivation on AV valve formation and function, we analyzed the number of AVC endothelial cells using *kdrl:nucGFP*. At 96 hpf, a reduced number of *kdrl:nucGFP*$^{+}$ cells was detected in the AVC region of *id2b*$^{-/-}$ embryos compared with *id2b*$^{+/+}$ (Supplementary Fig. S2a, b). In contrast, the number of atrial and ventricular endocardial cells did not differ between *id2b*$^{-/-}$ and *id2b*$^{+/+}$ (Supplementary Fig. S2c, d). Subsequently, we assessed hemodynamic flow by conducting time-lapse imaging of red blood cells labelled by *gata1:dsred*. Surprisingly, the pattern of hemodynamics was largely preserved in *id2b*$^{-/-}$ compared with *id2b*$^{+/+}$ siblings at 96 hpf (Supplementary Fig. S2e and videos). Additionally, we performed echocardiography to analyze blood flow in adult zebrafish as previously described[32]. In *id2b*$^{-/-}$ hearts, prominent retrograde blood flow was detected in the AVC region (8/13) (Fig. 4g), while unidirectional blood flow was observed in *id2b*$^{+/+}$ (10/10) (Fig. 4f). Quantification analysis showed ~32% retrograde blood flow in *id2b*$^{-/-}$, compared to 0% in *id2b*$^{+/+}$ zebrafish (Fig. 4h). Consistently, the superior and inferior leaflets were much thinner in *id2b*$^{-/-}$ exhibiting retrograde flow compared with control fish (data not shown). Overall, these histological and functional analyses indicate that *id2b* deletion leads to progressive defects in AV valve morphology and hemodynamic flow.

***id2b* deletion perturbs calcium signaling and contractile function in the myocardium**

Although similar defects in AV valve formation have been reported in both *klf2a* and *nfatc1* mutants, they do not display noticeable pericardial edema at the adult stage, nor do they experience early lethality[3,29,31-33]. Therefore, we sought to investigate whether other cardiac properties have also been affected by *id2b* loss-of-function. To this end, we employed RNA-seq analysis on purified embryonic *id2b*$^{-/-}$ and *id2b*$^{+/+}$ hearts (Supplementary Fig. S3). As expected, enrichment analysis of DEGs

demonstrated that the top-ranked anatomical structures affected by *id2b* deletion included the heart valve, the compact layer of ventricle, and the atrioventricular canal (Supplementary Fig. S3a). Interestingly, *id2b* inactivation also impacted phenotypes such as cardiac muscle contraction and heart contraction (Supplementary Fig. S3b). Therefore, we investigated cardiac contractile function through time-lapse imaging on the *myl7:mCherry* background. At 120 hpf, a significant decrease in cardiac contractility was observed in *id2b*$^{-/-}$, as evidenced by reduced fractional area change and heart rate, compared with *id2b*$^{+/+}$ (Fig. 5a-c). Similarly, echocardiography analysis showed that the contractile function in adult *id2b*$^{-/-}$ heart was dramatically reduced compared with age-matched *id2b*$^{+/+}$ (Fig. 5d, e). These functional defects in *id2b*-deleted hearts could not be attributed to differences in cardiomyocyte number, as we counted cardiomyocytes using the *myl7:H2A-mCherry* line and found no apparent changes between *id2b*$^{-/-}$ and *id2b*$^{+/+}$ embryos at 72 and 120 hpf (Supplementary Fig. S4a, b). Similarly, *id2b*$^{-/-}$ also developed regular trabecular structures at embryonic (Supplementary Fig. S4c) and adult stages (Fig. 4e). Through α-actinin immunostaining, we observed similar sarcomeric structures in 72 hpf and adult (115 dpf) *id2b*$^{-/-}$ and control cardiomyocytes (Supplementary Fig. S4d), corroborating that the reduced contractility in *id2b*-depleted heart was independent of structural defects.

The key functional unit that transmits electrical activity to contractile function is E-C coupling. Because *id2b*$^{-/-}$ displayed reduced cardiac function without conspicuous myocardial structural defects, we visualized calcium signaling in the developing heart using *actb2:GCaMP6s* zebrafish (Fig. 5g). Compared to *id2b*$^{+/+}$ control, *id2b*$^{-/-}$ exhibited markedly decreased calcium amplitude at 120 hpf (Fig. 5h), which is consistent with the reduced fractional area change. In cardiomyocyte, the entry of extracellular calcium is mainly mediated through the LTCC. As previously reported, a defect in zebrafish LTCC pore forming α1 subunit *cacna1c* leads to compromised cardiac function[24]. We collected hearts from 72 hpf and 5 months post-fertilization (mpf) zebrafish and detected downregulated *cacna1c* in *id2b*$^{-/-}$ compared to *id2b*$^{+/+}$ (Fig. 5i). In addition, we measured cardiac action potential using intracellular recording[34]. Compared to *id2b*$^{+/+}$ zebrafish, the duration of the action potential in *id2b*$^{-/-}$ was significantly shorter (Fig. 6j, k), consistent with the decreased expression level of *cacna1c*. Together, these data indicate that *id2b* loss-of-function leads to compromised calcium signaling and cardiac contractile function.

Reduced expression of *nrg1* mediates the compromised contractility in *id2b*$^{-/-}$

Because the deficiency of *id2b* in the endocardium disrupted the function of myocardium, we speculated that the crosstalk between these two types of cells was affected in *id2b*$^{-/-}$. Interestingly, comparing the differentially expressed genes in embryonic *id2b*$^{-/-}$ and *id2b*$^{+/+}$ hearts identified a significant reduction in the expression level of *nrg1*, a key mitogen regulating the intra-organ communications between endocardial cells and cardiomyocytes (Fig. 6a). Remarkably, analysis of a zebrafish single-cell database[35] revealed enriched expression of *nrg1* in endocardial cells (Supplementary Fig. S5). However, attempts to detect *nrg1* expression through in situ hybridization were unsuccessful, likely due to its low abundance in the heart. Alternatively, qRT-PCR analysis of purified 72 hpf embryonic hearts validated decreased *nrg1* levels in *id2b*$^{-/-}$ compared to control (Fig. 6b). Previous studies have demonstrated that perturbations in Nrg-Erbb2 signaling, as seen in zebrafish *erbb2* mutants, result in dysfunctional cardiac contractility[18]. Consistently, a decrease in heart rate was observed in embryos treated with the *erbb2* inhibitor AG1478 (Fig. 6e).

Remarkably, injecting *nrg1* mRNA at the 1-cell stage not only rescued the reduced expression of *cacna1c* in *id2b*$^{-/-}$ hearts (Fig. 6c) but also restored the diminished heart rate (Fig. 6d). This is consistent with prior study showing that Nrg1 administration can restore LTCC expression and calcium current in failing mammalian cardiomyocytes[36]. Overall, our data suggest that endocardial *id2b* promotes *nrg1* synthesis, thereby enhancing cardiomyocyte contractile function.

***id2b* interacts with *tcf3b* to limit its repressor activity on *nrg1* expression**

We further interrogated how *id2b* promotes the expression of *nrg1*. As a HLH factor lacking a DNA binding motif, *id2b* has been reported to form a heterodimer with *tcf3b* and inhibit its function. Notably, we detected expression of *tcf3b* in endocardial cells by analyzing a zebrafish single-cell database[35] (Supplementary Fig. S6). To determine whether this interaction occurs in zebrafish, Flag-*id2b* and HA-*tcf3b* were co-expressed in HEK293 cells. Co-immunoprecipitation analysis confirmed the direct binding of *id2b* to *tcf3b* protein (Fig. 7a). qRT-PCR analysis on purified 72 hpf embryonic hearts revealed a significant increase in the expression of *socs3b* and *socs1a*, target genes of *tcf3b*, in *id2b*$^{-/-}$

compared to *id2b*$^{+/+}$ (Fig. 7b). This suggests an elevation in *tcf3b* activity associated with the loss of *id2b* function. Notably, the expression levels of *tcf3a* and *tcf3b* remained consistent between *id2b*$^{-/-}$ and *id2b*$^{+/+}$ hearts (Fig. 7b).

To understand how the altered interaction between *id2b* and *tcf3b* influences *nrg1* expression, we analyzed the promoter region of zebrafish *nrg1* using JASPAR and identified two potential *tcf3b* binding sites (Fig. 7c). Subsequently, a DNA fragment containing the zebrafish *nrg1* promoter region was subcloned into a vector carrying the luciferase reporter gene. Co-injection of this construct with *tcf3b* mRNA into 1-cell stage embryos resulted in a significant decrease in luciferase signal. Conversely, co-injection with a previously characterized *tcf3b* morpholino led to enhanced luciferase intensity (Fig. 7d). These results suggest a possible mechanism by which *tcf3b* represses *nrg1* expression in zebrafish.

Lastly, injecting *tcf3b* morpholino into *id2b*$^{-/-}$ embryos was performed to assess whether attenuating the overactive *tcf3b* in *id2b*$^{-/-}$ could restore the expression level of *nrg1*. qRT-PCR analysis of purified 72 hpf hearts revealed a partial restoration of the diminished *nrg1* expression in *id2b*$^{-/-}$ upon *tcf3b* inhibition (Fig. 7e). Taken together, our results indicate that biomechanical cues activate endocardial *id2b* expression, leading to its interaction with *tcf3b* to alleviate repression on the *nrg1* promoter. Consequently, the depletion of *id2b* unleashes *tcf3b*'s repressor activity, leading to a reduction in *nrg1* expression, which further acts through *erbb2* to regulate cardiomyocyte function (Fig. 7f).

Discussion

Biomechanical forces play an essential role in regulating the patterning and function of the heart. At AVC, oscillatory flow promotes the expression of *klf2a* and *nfatc1* to modulate valve morphogenesis. In chamber endocardium, blood flow induces endocardial cells to acquire distinct cell morphology. However, it still lacks a systematic analysis of the transcriptome underlying compromised heartbeats. In the present study, we analyzed embryonic zebrafish hearts without contractility and identified genes that are regulated by biomechanical forces. Specifically, our results unveiled the endocardial-specific expression of *id2b*, which was tightly regulated by flow-sensitive primary cilia-*klf2* axis. Genetic

deletion of *id2b* resulted in compromised valve formation and progressive atrium enlargement. In addition, a reduction in heart rate and contractile force was observed in *id2b*$^{-/-}$, owing to decreased expression of LTCC α1 subunit *cacna1c*. Mechanistically, *id2b* interacts with bHLH transcription factor *tcf3*b to limit its repressor activity. Hence genetic deletion of *id2b* unleashes *tcf3*b activity, which further represses endocardial *nrg1* expression. As a result, Injection of *nrg1* mRNA partially rescues the phenotype of *id2b* deletion. Overall, our findings identify *id2b* as a novel mediator that regulate the interplay between endocardium and myocardium during heart development.

In mammals, the deletion of *Id2* leads to malformations in the arterial and venous poles of the heart, as well as affects AV valve morphogenesis[37,38]. Interestingly, approximately 20% perinatal lethality is reported in *Id2* knockout mice, exhibiting AV septal defects and membranous ventricular septal defects[37]. Remarkably, pericardial edema is evident in 20% of adult *id2b*$^{-/-}$ zebrafish, with a prominent enlargement of the atrium. The superior and inferior leaflets of AV valves in *id2b*$^{-/-}$ mutants are significantly thinner compared to the control. Therefore, our results suggest that *id2b* may play a similar role in regulating AV valve formation in zebrafish as its mammalian orthologue *Id2*. It is proposed that the loss of *Id2* in mice results in compromised endocardial proliferation and aberrant endothelial-to mesenchymal transformation (EMT), collectively leading to defective valve morphogenesis[37]. Nevertheless, the mechanism by which *id2b* loss-of-function causes a reduction in leaflet thickness in zebrafish remains to be determined in future studies.

id2b has been recognized as a target gene of the BMP signaling pathway. As expected, knockdown of *bmp2b*, *bmp4*, and *bmp7a* at 1-cell stage confirms that endocardial *id2b* expression is controlled by BMP activity during early embryonic development. Surprisingly, treatment with the BMP inhibitor Dorsomorphin at 24 and 36 hpf, when cardiac contractions have already initiated, fails to alter *id2b* expression in the endocardium, suggesting that BMP is dispensable for *id2b* activation at these stages. Instead, endocardial *id2b* expression is reduced upon loss-of-function of *klf2a*, *klf2b*, and *ift88*, suggesting an essential role of the primary cilia-*klf2* axis in mediating *id2b* activation. In endocardial cells, Trp, Piezo, and ATP-dependent P2X/P2Y channels[4,6,39,40] are well-established sensors for biomechanical stimulation. The activation of these channels further promotes the activities of Klf2 and

Nfatc1 to drive heart development and valvulogenesis. However, whether these channels are also required for the activation of *id2b* warrants further investigation.

The Nrg-Erbb signaling plays an essential role in regulating heart morphogenesis and function. In the mammalian heart, the genetic deletion of Nrg1 or Erbb2 results in severely perturbed cardiac trabeculae formation[13-15]. Zebrafish *erbb2* mutants exhibit a similar defect in cardiomyocyte proliferation and trabeculation[18]. Interestingly, *nrg1* mutant zebrafish display grossly normal cardiac structure during early embryonic devolpment[19,41]. Nevertheless, zebrafish *nrg2a* loss-of-function leads to defective trabeculae formation, suggesting that *nrg2a* is the predominant ligand secreted from endocardium, promoting ventricular morphogenesis[19]. In the adult stage, perivascular cells[42] or regulatory T cells[43]-derived *nrg1* promotes cardiomyocyte proliferation during heart regeneration. Hence, the specific ligand/receptor and the spatiotemporal regulation of the Nrg-Erbb axis appear to be more complicated in both embryonic and adult zebrafish. Interestingly, the *nrg1* mutant heart exhibits a defect in cardiac nerve expansion and heart maturation at the juvenile stage despite normal cardiac structure formation[41], suggesting its potential role in regulating cardiac function. Our findings demonstrate that the expression of *nrg1* in embryonic endocardial cells is influenced by biomechanical cues and *id2b* activity. This signaling axis is essential for coordinating endocardium-myocardium interaction and establishing proper cardiac function.

Materials and methods

Zebrafish handling and lines

All animal procedures were approved by the Animal Care and Use Committee of the Zhejiang University School of Medicine. Embryonic and adult fish were raised and maintained under standard conditions at 28 °C on a 14/10 hour day/night cycle. The following zebrafish lines were used in this study: *Tg(myl7:mCherry)*^{sd7} [44], *Tg(myl7:H2A-mCherry)*^{sd12} [45], *Tg(kdrl:mCherry)*^{S896} [46], *Tg(kdrl: nucGFP)*^{y7} [47], *Tg(Bre:d2GFP)*^{mw30} [48], and *Tg(actb2:Gcamp6s).* To generate the *id2b* mutant, two short guide RNAs (sgRNAs) targeting exon 1 were generated using the MAXIscript T7 transcription kit (ambion, AM1314). The sgRNAs were as follows: sgRNA1: 5’ - GAAGGCAGTCAGTCCGGTG - 3’; sgRNA2: 5’ - GAACCGGAGCGTGAGTAAGA - 3’. The two sgRNAs, along with zCas9 protein,

were co-injected into one-cell stage embryos. Embryos were raised to adulthood and crossed to wild-type zebrafish to obtain F_1 progenies. Through PCR analysis, a mutant line with a 157 bp truncation was identified.

The knock-in *id2b:eGFP* line was generated using a previously reported method[27]. Briefly, three sgRNAs were designed to target the intron of *id2b* (sgRNA1: 5' - GAGACAAATATCTACTAGTG - 3'; sgRNA2: 5' - GTTGAACACATGACGATATT - 3'; sgRNA3: 5' - GCACAACTTAGATTTCAAGT - 3'). Co-injection of each individual sgRNA with zCas9 protein into one-cell stage zebrafish embryos yielded varying cleavage efficiency. Since sgRNA2 displayed the highest gene editing efficiency, it was selected for subsequent studies. Next, a donor plasmid containing the sgRNA targeting sequence of the intron, exon 2 of *id2b*, and P2A-eGFP was generated. Co-injection of sgRNA, donor plasmid, and zCas9 protein into one-cell stage embryos led to concurrent cleavage of the sgRNA targeting sites in both the zebrafish genome and the donor plasmid (Fig. 2a). Accordingly, eGFP fluorescence was observed in injected 24 hpf zebrafish embryos, indicating the incorporation of the donor. The insertion of the *id2b*-p2A-eGFP donor into the genome was confirmed by PCR analysis with primers recognizing target site or donor sequences, respectively (Fig. 2a). Embryos with mosaic eGFP expression were raised to adulthood and crossed with wild-type zebrafish to obtain F_1 progenies. Overall, two founders were identified. The junction region of the F_1 embryos was sequenced to determine the integration sites. Although the two founders had slightly different integration sites in the intron, the expression pattern and fluorescence intensity of eGFP were indistinguishable between the two lines.

Morpholinos

All morpholinos (Gene Tools) used in this study have been previously characterized. *tnnt2a* MO (5' - CATGTTTGCTCTGATCTGACACGCA - 3')[49]; *ift88* MO (5' - CTGGGACAAGATGCACATTCTCCAT - 3')[29]; *bmp2b* MO (5' - ACCACGGCGACCATGATCAGTCAGT - 3')[50]; *bmp4* MO (5' - AACAGTCCATGTTTGTCGAGAGGTG - 3')[51]; *bmp7a* MO (5' - GCACTGGAAACATTTTTAGAGTCAT - 3')[50]; *tcf3b* MO (5' -

CGCCTCCGTTAAGCTGCGGCATGTT - 3')[52]. For each morpholino, a 1 nl solution was injected into one-cell stage embryos at the specified concentrations: 0.5 ng *tnnt2a* MO, 2 ng *ift88* MO, 0.5 ng *bmp2b* MO, 2 ng *bmp4* MO, 4 ng *bmp7a* MO, and 1 ng *tcf3b* MO.

Small molecules treatment

To inhibit cardiac contraction, embryos were incubated in 1 mg/mL tricaine (Sigma, A5040) or 10 uM blebbistatin (MedChemExpress, HY13441) PTU-added egg water for 12-24 hours. In order to inhibit *erbb2* signaling pathway, 10 uM AG1478 (Sigma, 658552) were used to treat 4 dpf larvae. To inhibit BMP signaling pathway, 10 uM Dorsomorphin (Sigma, P5499) was used to treat 24 and 36 hpf embryos.

***In situ* hybridization**

Whole mount *in situ* hybridization was performed as previously described[34]. The probes were synthesized using the DIG RNA labeling kit (Roche). The primers used for obtaining the *id2b* probe template were as follows: Forward 5' - ATGAAGGCAGTCAGTCCGGTGAGGT - 3'; Reverse 5' - TCAACGAGACAGGGCTATGAGGTCA - 3'.

Embryonic heart isolation and RNA-seq analysis

Hearts were isolated from embryos carrying the *Tg*(*myl7: mCherry)* transgene following an established protocol[26]. A minimum of 1,000 hearts for each experimental group were manually collected under a Leica M165FC fluorescence stereomicroscope and transferred into ice-cold PBS buffer. After centrifugation at 12, 000 g for 2 min at 4°C, the supernatant was removed, and hearts were lysed in cold Trizol buffer (Ambion, 15596). Total RNA was extracted for subsequent quantitative real-time PCR or RNA-seq analysis.

Duplicate samples from control and Tricaine-treated embryonic hearts underwent RNA-seq. Raw sequencing reads were preprocessed to remove adapters and filter low-quality reads. Clean sequencing reads were then mapped to the zebrafish reference[53] using STAR with default parameters[54]. Subsequently, gene quantification was carried out with RSEM[55]. The gene expected count was applied

to identify differential expression genes (DEGs), retaining only genes with counts per million (CPM) of 10 in at least two samples. DESeq2[56] was employed for differential expression analysis, and *P*-values were adjusted using BH correction. DEGs were defined as those with $|\log_2 \text{fold change}| \geq 0.585$ and an adjusted *P*-value < 0.1. The primary focus was on genes related to transcription regulation, and gene enrichment analysis was conducted using ClusterProfiler[57]. To analyze DEGs in *id2b*$^{-/-}$ and control embryonic hearts, we performed enrichment analysis with the R package EnrichR, dissecting the potential anatomy expression pattern and underlying phenotypes. We mainly focused on genes with the heart related phenotypes, including cardiac muscle tissue development, cardiomyocyte differentiation, heart morphogenesis and cardiac chamber development. All the analysis on identifying DEGs were batch corrected.

Quantitative real-time PCR analysis

After extraction from isolated embryonic hearts, 50 ng-1 ug of mRNA was reverse transcribed to cDNA using the PrimeScript RT Master Mix kit (Takara, RR036A). Real-time PCR was performed using the TB Green Premix Ex Taq kit (Takara, RR420A) on the Roche LightCycler 480. Expression levels of the target genes were normalized to *actb1* as an internal control. All experiments were repeated three times. The following primer sets were used: *id2b* Forward 5' - ACCTTCAGATCGCACTGGAC - 3', Reverse 5' - CTCCACGACCGAAACACCATT - 3'; *nrg1* Forward 5' - CTGCATCATGGCTGAGGTGA - 3', Reverse 5' - TTAACTTCGGTTCCGCTTGC - 3'; *cacnα1c* Forward 5' - GCCCTTATTGTAGTGGGTAGTG - 3', Reverse 5' - AGTGTTTTGGAGGCCCATTG - 3'; *tcf3a* Forward 5' - CCTCCGGTCATGAGCAACTT - 3', Reverse 5' - TTTCCCATGATGCCTTCGCT - 3'; *tcf3b* Forward 5' - CCTTTAATGCGCCGTGCTTC - 3', Reverse 5' - GCGTTCTTCCATTCCTGTACCA - 3'; *socs1a* Forward 5' - TCAGCCTGACAGGAAGCAAG - 3', Reverse 5' - GTTGCACAGGGATGCAGTCG - 3'; *socs3b* Forward 5' - GGGACAGTGAGTTCCTCCAA - 3', Reverse 5' - ATGGGAGCATCGTACTCCTG - 3'; *actb1* Forward 5' - ACCACGGCCGAAAGAGAAAT - 3', Reverse 5' - GCAAGATTCCATACCCAGGA - 3'.

Co-immunoprecipitation (Co-IP) and western blot

Zebrafish *tcf3b* and *id2b* were overexpressed in 293T cell for 48 hours. The transfected cells were then collected and lysed using IP lysis buffer (Sangon Biotech, C500035) containing protease and phosphatase inhibitors (Sangon Biotech, C510009, C500017). For the IP experiment, anti-Flag antibody (Cell Signaling Technology, 14793, 1:100) was incubated with cell lysates overnight at 4°C. Pretreated magnetic beads were bound with the antigen-antibody complex for 4 hours at 4°C, followed by washing with IP lysis buffer three times. For western blot, samples were denatured at 95°C for 10 min, separated on a 5%-12% gradient gel. Proteins were then transferred to a PVDF membrane (Sigma, ISEQ00010). The membrane was blocked for 1 hour with 5% nonfat milk or 5% BSA (Sangon Biotech) dissolved in TBST and then incubated with primary antibodies (anti-FLAG, Cell Signaling Technology, 14793, 1:1000; anti-HA, Sigma, H3663, 1:1000) overnight at 4°C, followed by three 10-min TBST washes. HRP-conjugated secondary antibodies (Invitrogen, 31430, 31460) were incubated for 1 hour at room temperature, followed by three 10-min TBST washes. The detection of immunoreactive bands was performed with a chemiluminescent substrate (Thermo Scientific, 34577) and imaged using the Azure Biosystems 400.

Immunofluorescence

For immunofluorescence on adult zebrafish hearts, we fixed the hearts overnight in 4% paraformaldehyde at 4 °C, followed by equilibration through 15% and 30% sucrose in PBS solution. The hearts were embedded and frozen in O.C.T. compound (Epredia, 6502), and 10 μm thick cryosections were prepared using a CryoStar NX50 cryostat. Immunofluorescence experiments were performed as previously described[58]. For immunofluorescence on embryonic hearts, embryos were fixed overnight in 4% paraformaldehyde at 4°C, washed twice quickly in 100% methanol, and then dehydrated overnight at -20°C in 100% methanol. Subsequently, rehydration was performed through a methanol gradient (100%, 75%, 50%, 25%, 10 min each), followed by three washes in PBST (1% PBS/0.1% Triton-X100, 10 min each). The embryos were treated with 10 μg/mL proteinase K diluted in PBST for 20 min at room temperature, re-fixed in 4% paraformaldehyde for 20 min, washed in PBST, and immersed in blocking solution (PBST/1% BSA/2% goat serum) for 1 hour at room

temperature. Following this, the embryos were incubated in the primary antibody diluted in blocking solution overnight at 4°C. After washing in PBST, they were incubated in the secondary antibody (1:200) for 2 hours at room temperature. The primary antibody used was: Anti-GFP antibody (Santa Cruz Biotechnology, sc9996, 1: 200), anti-α-actinin antibody (Sigma, A7811, 1: 200). The secondary antibody used was: Anti-mouse IgG-Alexa 488 (Invitrogen, A11011, 1: 400). DAPI was used to stain cell nuclei.

Cardiac function analysis

To assess cardiac function in embryonic hearts, embryos were embedded in 1% low melting agarose, and heart contractions were recorded for 1 min using a Nikon Ti2 microscope at a rate of 25 frames per second. Fractional shortening and heart rate were measured as described previously[34]. For cardiac contractile functions in adulthood, zebrafish were fixed on a sponge soaked with system water with the belly facing up and echocardiography was performed[59]. Videos and images in color Doppler mode and B-mode were obtained using the Vevo1100 imaging system at a frequency of 50 MHz. Nikon NIS elements AR analysis and Image J software were employed for data extraction. To evaluate AV valve function, the ratio of inflow and outflow area in the same frame was quantified[32].

Calcium imaging

At 120 hpf, embryos were treated with 10 mM 2,3-butanedione monoxime (BDM, Sigma, B0753) and mounted in 1% low melting agarose. Time-lapse images were acquired using a Nikon Ti2 microscope at a rate of 50 frames per second. Data were analyzed using Nikon NIS elements AR analysis software.

Intracellular action potential recording

Electrophysiology study was performed on adult zebrafish ventricles as previously described[34]. Briefly, hearts were mounted in a chamber containing Tyrode's solution: NaCl 150 mM, KCl 5.4 mM, $MgSO_4$ 1.5 mM, NaH_2PO_4 0.4 mM, $CaCl_2$ 2 mM, Glucose 10 mM, HEPES 10 mM, pH was adjusted to 7.4. Glass pipettes with tip resistance 30-40 MΩ were filled with 3M KCl solution. Intracellular action potentials were recorded using an HEKA amplifier and pClamp10.3 software (Molecular Devices).

Histology and HE staining

Adult hearts were dissected and fixed overnight at 4°C in 4% PFA, followed by three PBS washes. Dehydration involved an ethanol gradient (70%, 80%, 95%, 100%, 100%, 30 min each), followed by three soaks in dimethylbenzene at 65°C, before embedding in paraffin. Sections of 5 um thickness were prepared using the Leica RM2235 manual rotary microtome for hematoxylin and eosin (HE) staining.

Injection of mRNA

The embryonic zebrafish cDNA library was used as a template to amplify the *nrg1* and *tcf3b* fragment, which was then subcloned into the pCS2 vector. The vector was linearized using Not I restriction endonuclease, and mRNA was transcribed in vitro using the mRNA transcription kit (Ambion, AM1340). 100 pg of purified mRNA was injected into one-cell stage embryos.

Luciferase assay

The LCR (luciferase reporter) plasmid was generated by subcloning the 5′ UTR of *nrg1* into the upstream region of renilla luciferase on the psiCheck2 plasmid. Following construction, 25 pg of the LCR plasmid was co-injected with either 100 pg of *tcf3b* mRNA or 1 ng of *tcf3b* MO into 1-cell stage zebrafish embryos. At 48 hpf, twenty embryos were gathered into one group and fully lysed. Subsequently, firefly and renilla luciferase activities were sequentially measured using a microplate reader with the dual luciferase reporter gene assay kit (Yeasen, 11402ES60), according to the manufacturer′s instructions. The experiment was independently replicated three times. The relative renilla luciferase activity, normalized by firefly luciferase activity, served as an indicator of *nrg1* expression level under the influence of *tcf3b* overexpression or reduction.

Image processing and statistical analysis

Whole mount *in situ* hybridization images were captured with a Leica M165FC stereomicroscope. Live imaging of zebrafish embryos involved mounting anesthetized embryos in 1% low melting agarose (Sangon Biotech, A600015) and manually oriented them for optimal visual access to the heart.

Confocal images were obtained with a Nikon Ti2 confocal microscope. Fluorescence intensity and cell number counting were processed using Nikon NIS Elements AR analysis and Image J software. Statistical analysis was performed using Graphpad prism 8 software. No statistical methods were used to predetermine sample size. Unpaired two-tailed Student's t-tests was used to determine statistical significance. Data are presented as mean ± s.e.m, $*P < 0.05$ was considered to be statistically significant.

Acknowledgements: We thank Dr. Pengfei Xu for providing morpholinos. We also thank Dr. Jia Li for the support in generating the *id2b:eGFP* line.

Author Contributions: Shuo Chen and Peidong Han contributed to the study design. Shuo Chen, Jinxiu Liang, Weijia Zhang, Peijun Jiang, Wenyuan Wang, Xiaoying Chen and Yuanhong Zhou conducted experiments. Jie Yin analyzed RNA-sequencing data. Peng Xia, Fan Yang, Ying Gu, and Ruilin Zhang provided key reagents and analytic tool. Shuo Chen, Jie Yin, and Peidong Han prepared the manuscript.

Source of Funding: This work was supported by the National Key R&D Program of China (2018YFA0800102, 2023YFA1800602, 2018YFA0800501), and the National Natural Science Foundation of China (32170823, 31871462).

Disclosures: The authors declare that they have no conflict of interest.

References

1 Duchemin, A. L., Vignes, H., Vermot, J. & Chow, R. Mechanotransduction in cardiovascular morphogenesis and tissue engineering. *Curr Opin Genet Dev* **57**, 106-116 (2019).

2 Sidhwani, P. & Yelon, D. Fluid forces shape the embryonic heart: Insights from zebrafish. *Curr Top Dev Biol* **132**, 395-416 (2019).

557 3 Vermot, J. *et al.* Reversing blood flows act through klf2a to ensure normal
558 valvulogenesis in the developing heart. *PLoS Biol* **7**, e1000246 (2009).
559 4 Heckel, E. *et al.* Oscillatory Flow Modulates Mechanosensitive klf2a Expression
560 through trpv4 and trpp2 during Heart Valve Development. *Curr Biol* **25**, 1354-1361
561 (2015).
562 5 Galvez-Santisteban, M. *et al.* Hemodynamic-mediated endocardial signaling controls
563 in vivo myocardial reprogramming. *Elife* **8** (2019).
564 6 Fukui, H. *et al.* Bioelectric signaling and the control of cardiac cell identity in
565 response to mechanical forces. *Science* **374**, 351-354 (2021).
566 7 Dietrich, A. C., Lombardo, V. A., Veerkamp, J., Priller, F. & Abdelilah-Seyfried, S.
567 Blood flow and Bmp signaling control endocardial chamber morphogenesis. *Dev Cell*
568 **30**, 367-377 (2014).
569 8 Sidhwani, P. *et al.* Cardiac function modulates endocardial cell dynamics to shape
570 the cardiac outflow tract. *Development* **147** (2020).
571 9 Staudt, D. W. *et al.* High-resolution imaging of cardiomyocyte behavior reveals two
572 distinct steps in ventricular trabeculation. *Development* **141**, 585-593 (2014).
573 10 Peshkovsky, C., Totong, R. & Yelon, D. Dependence of cardiac trabeculation on
574 neuregulin signaling and blood flow in zebrafish. *Dev Dyn* **240**, 446-456 (2011).
575 11 Auman, H. J. *et al.* Functional modulation of cardiac form through regionally
576 confined cell shape changes. *PLoS Biol* **5**, e53 (2007).
577 12 Lin, Y. F., Swinburne, I. & Yelon, D. Multiple influences of blood flow on
578 cardiomyocyte hypertrophy in the embryonic zebrafish heart. *Dev Biol* **362**, 242-253
579 (2012).
580 13 Gassmann, M. *et al.* Aberrant neural and cardiac development in mice lacking the
581 ErbB4 neuregulin receptor. *Nature* **378**, 390-394 (1995).
582 14 Lee, K. F. *et al.* Requirement for neuregulin receptor erbB2 in neural and cardiac
583 development. *Nature* **378**, 394-398 (1995).
584 15 Meyer, D. & Birchmeier, C. Multiple essential functions of neuregulin in
585 development. *Nature* **378**, 386-390 (1995).
586 16 Lai, D. *et al.* Neuregulin 1 sustains the gene regulatory network in both trabecular
587 and nontrabecular myocardium. *Circ Res* **107**, 715-727 (2010).
588 17 Rentschler, S. *et al.* Neuregulin-1 promotes formation of the murine cardiac
589 conduction system. *Proc Natl Acad Sci U S A* **99**, 10464-10469 (2002).
590 18 Liu, J. *et al.* A dual role for ErbB2 signaling in cardiac trabeculation. *Development* **137**,
591 3867-3875 (2010).
592 19 Rasouli, S. J. & Stainier, D. Y. R. Regulation of cardiomyocyte behavior in zebrafish
593 trabeculation by Neuregulin 2a signaling. *Nat Commun* **8**, 15281 (2017).
594 20 Han, P. *et al.* Coordinating cardiomyocyte interactions to direct ventricular chamber
595 morphogenesis. *Nature* **534**, 700-704 (2016).
596 21 Guo, Y. & Pu, W. T. Cardiomyocyte Maturation: New Phase in Development. *Circ Res*
597 **126**, 1086-1106 (2020).
598 22 Alvarez-Dominguez, J. R. & Melton, D. A. Cell maturation: Hallmarks, triggers, and
599 manipulation. *Cell* **185**, 235-249 (2022).

600 23 Bers, D. M. Cardiac excitation-contraction coupling. *Nature* **415**, 198-205 (2002).
601 24 Rottbauer, W. *et al.* Growth and function of the embryonic heart depend upon the
602 cardiac-specific L-type calcium channel alpha1 subunit. *Dev Cell* **1**, 265-275 (2001).
603 25 Samsa, L. A. *et al.* Cardiac contraction activates endocardial Notch signaling to
604 modulate chamber maturation in zebrafish. *Development* **142**, 4080-4091 (2015).
605 26 Burns, C. G. & MacRae, C. A. Purification of hearts from zebrafish embryos.
606 *Biotechniques* **40**, 274, 276, 278 passim (2006).
607 27 Li, J. *et al.* Intron targeting-mediated and endogenous gene integrity-maintaining
608 knockin in zebrafish using the CRISPR/Cas9 system. *Cell Res* **25**, 634-637 (2015).
609 28 Forster, D. *et al.* Genetic targeting and anatomical registration of neuronal
610 populations in the zebrafish brain with a new set of BAC transgenic tools. *Sci Rep* **7**,
611 5230 (2017).
612 29 Li, X. *et al.* Primary cilia mediate Klf2-dependant Notch activation in regenerating
613 heart. *Protein Cell* **11**, 433-445 (2020).
614 30 Nauli, S. M. *et al.* Endothelial cilia are fluid shear sensors that regulate calcium
615 signaling and nitric oxide production through polycystin-1. *Circulation* **117**, 1161-
616 1171 (2008).
617 31 Rasouli, S. J. *et al.* The flow responsive transcription factor Klf2 is required for
618 myocardial wall integrity by modulating Fgf signaling. *Elife* **7** (2018).
619 32 Gunawan, F., Gentile, A., Gauvrit, S., Stainier, D. Y. R. & Bensimon-Brito, A. Nfatc1
620 Promotes Interstitial Cell Formation During Cardiac Valve Development in Zebrafish.
621 *Circ Res* **126**, 968-984 (2020).
622 33 Novodvorsky, P. *et al.* klf2ash317 Mutant Zebrafish Do Not Recapitulate Morpholino-
623 Induced Vascular and Haematopoietic Phenotypes. *PLoS One* **10**, e0141611 (2015).
624 34 Zhang, R. *et al.* In vivo cardiac reprogramming contributes to zebrafish heart
625 regeneration. *Nature* **498**, 497-501 (2013).
626 35 Jiang, M. *et al.* Characterization of the Zebrafish Cell Landscape at Single-Cell
627 Resolution. *Front Cell Dev Biol* **9**, 743421 (2021).
628 36 Wang, X. *et al.* Neuregulin-1beta Partially Improves Cardiac Function in Volume-
629 Overload Heart Failure Through Regulation of Abnormal Calcium Handling. *Front*
630 *Pharmacol* **10**, 616 (2019).
631 37 Moskowitz, I. P. *et al.* Transcription factor genes Smad4 and Gata4 cooperatively
632 regulate cardiac valve development. [corrected]. *Proc Natl Acad Sci U S A* **108**, 4006-
633 4011 (2011).
634 38 Jongbloed, M. R. *et al.* Expression of Id2 in the second heart field and cardiac defects
635 in Id2 knock-out mice. *Dev Dyn* **240**, 2561-2577 (2011).
636 39 Li, J. *et al.* Piezo1 integration of vascular architecture with physiological force.
637 *Nature* **515**, 279-282 (2014).
638 40 Nonomura, K. *et al.* Mechanically activated ion channel PIEZO1 is required for
639 lymphatic valve formation. *Proc Natl Acad Sci U S A* **115**, 12817-12822 (2018).
640 41 Brown, D. *et al.* Neuregulin-1 is essential for nerve plexus formation during cardiac
641 maturation. *J Cell Mol Med* **22**, 2007-2017 (2018).

642 42 Gemberling, M., Karra, R., Dickson, A. L. & Poss, K. D. Nrg1 is an injury-induced
643 cardiomyocyte mitogen for the endogenous heart regeneration program in zebrafish.
644 *Elife* **4** (2015).
645 43 Hui, S. P. *et al.* Zebrafish Regulatory T Cells Mediate Organ-Specific Regenerative
646 Programs. *Dev Cell* **43**, 659-672 e655 (2017).
647 44 Palencia-Desai, S. *et al.* Vascular endothelial and endocardial progenitors
648 differentiate as cardiomyocytes in the absence of Etsrp/Etv2 function. *Development*
649 **138**, 4721-4732 (2011).
650 45 Schumacher, J. A., Bloomekatz, J., Garavito-Aguilar, Z. V. & Yelon, D. tal1 Regulates
651 the formation of intercellular junctions and the maintenance of identity in the
652 endocardium. *Dev Biol* **383**, 214-226 (2013).
653 46 Chi, N. C. *et al.* Foxn4 directly regulates tbx2b expression and atrioventricular canal
654 formation. *Genes Dev* **22**, 734-739 (2008).
655 47 Roman, B. L. *et al.* Disruption of acvrl1 increases endothelial cell number in zebrafish
656 cranial vessels. *Development* **129**, 3009-3019 (2002).
657 48 Collery, R. F. & Link, B. A. Dynamic smad-mediated BMP signaling revealed through
658 transgenic zebrafish. *Dev Dyn* **240**, 712-722 (2011).
659 49 Sehnert, A. J. *et al.* Cardiac troponin T is essential in sarcomere assembly and cardiac
660 contractility. *Nat Genet* **31**, 106-110 (2002).
661 50 Lele, Z., Bakkers, J. & Hammerschmidt, M. Morpholino phenocopies of the swirl,
662 snailhouse, somitabun, minifin, silberblick, and pipetail mutations. *Genesis* **30**, 190-
663 194 (2001).
664 51 Weber, S. *et al.* SIX2 and BMP4 mutations associate with anomalous kidney
665 development. *J Am Soc Nephrol* **19**, 891-903 (2008).
666 52 Dorsky, R. I., Itoh, M., Moon, R. T. & Chitnis, A. Two tcf3 genes cooperate to pattern
667 the zebrafish brain. *Development* **130**, 1937-1947 (2003).
668 53 Weinberger, M., Simões, F. C., Patient, R., Sauka-Spengler, T. & Riley, P. R. Functional
669 Heterogeneity within the Developing Zebrafish Epicardium. *Dev Cell* **52**, 574-
670 590.e576 (2020).
671 54 Dobin, A. *et al.* STAR: ultrafast universal RNA-seq aligner. *Bioinformatics* **29**, 15-21
672 (2013).
673 55 Li, B. & Dewey, C. N. RSEM: accurate transcript quantification from RNA-Seq data
674 with or without a reference genome. *BMC Bioinformatics* **12**, 323 (2011).
675 56 Love, M. I., Huber, W. & Anders, S. Moderated estimation of fold change and
676 dispersion for RNA-seq data with DESeq2. *Genome Biology* **15**, 550 (2014).
677 57 Wu, T. *et al.* clusterProfiler 4.0: A universal enrichment tool for interpreting omics
678 data. *The Innovation* **2**, 100141 (2021).
679 58 Han, P. *et al.* Hydrogen peroxide primes heart regeneration with a derepression
680 mechanism. *Cell Res* **24**, 1091-1107 (2014).
681 59 Wang, L. W. *et al.* Standardized echocardiographic assessment of cardiac function in
682 normal adult zebrafish and heart disease models. *Dis Model Mech* **10**, 63-76 (2017).

683

Figure legends

Figure 1. Identification of *id2b* as a blood flow sensitive gene.

(**a**) Schematic showing the experimental procedures, including treatment, heart collection, and RNA-sequencing of zebrafish embryonic hearts. (**b**) KEGG enrichment analysis depicting differentially expressed genes encoding transcription factors and transcriptional regulators between control (ctrl) and tricaine-treated embryonic hearts. Red and blue rectangles represent up-regulated and down-regulated gene sets, respectively. $|\log_2 \text{fold change}| \geq 0.585$, adjusted p-value<0.1. Each replicate contains approximately 1,000 hearts. (**c**) Heat map exhibiting representative genes from KEGG pathways mentioned in (**b**). (**d**) qRT-PCR analysis of *id2b* mRNA in control and tricaine-treated embryonic hearts. Data were normalized to the expression of *actb1*. Each sample contains ~1,000 embryonic hearts. (**e**) *In situ* hybridization of *id2b* in 72 hpf and 96 hpf ctrl, tricaine (1 mg/mL), and blebbistatin (10 μM)-treated embryos. Numbers at the bottom of each panel indicate the ratio of representative staining. (**f**) *In situ* hybridization showing reduced *id2b* expression in *tnnt2a* morpholino-injected embryos at 72 hpf compared to control. *** p<0.001. Scale bars: 50 μm.

Figure 2. The spatiotemporal expression of *id2b*.

(**a**) Schematic of the intron targeting-mediated *eGFP* knockin at the *id2b* locus using the CRISPR-Cas9 system. The sgRNA targeting sequence and the protospacer adjacent motif (PAM) sequence are shown in orange and blue, respectively. The donor plasmid comprises left and right arm sequences and a *linker-FLAG-P2A-eGFP* cassette denoted by black lines with double arrows and green box, respectively. The *linker-FLAG-P2A-eGFP* cassette was integrated into the *id2b* locus upon co-injection of the donor plasmid with sgRNA and zCas9 protein, enabling detection by PCR using two pairs of primers (F1, R1 and F2, R2)-the former length yielding a length of about 2.2 kb and the latter about 2.7 kb. (**b**) Zebrafish *id2b* expression pattern, as indicated by in situ hybridization of embryos at designated time points, was consistent with the fluorescence localization of *id2b:eGFP*, revealing expression in the heart, brain, retina, notochord, pronephric duct, and other tissues. (**c**) Three dimensional (3D) reconstructions (top) and confocal sections (bottom) of *id2b:eGFP; Tg(myl7:mCherry)* hearts at designated time points. (**d**) 3D reconstructions (top) and confocal sections

(bottom) of *id2b:eGFP; Tg(kdrl:mCherry)* embryos at specific time points. Magenta: *id2b:eGFP*; yellow: *kdrl:mCherry*. (**e**) Confocal z-stack maximal intensity projection of *id2b:eGFP;Tg(kdrl:mCherry*) embryos at 96 hpf showing the whole body (lateral view) and the head (top view). (**f**) Immunofluorescence of adult *id2b:eGFP; Tg(kdrl:mCherry*) heart section (middle panel). Enlarged views of boxed areas are shown in the left and right panels. Green: eGFP; red: mCherry; blue, DAPI. Scale bars: 500 μm (**b**, **e**, left and **f**); 100 μm (**e**, right); 50 μm (**c** and **d**).

Figure 3. Cardiac contraction promotes endocardial *id2b* expression through primary cilia.

(**a**) Representative confocal z-stack (maximal intensity projection) of *id2b:eGFP* embryos under different conditions: control, tricaine-treated, blebbistatin-treated, and *tnnt2a* morpholino-injected. (**b**) Quantification of mean fluorescence intensity (MFI) of *id2b:eGFP* in the working myocardium (atrium and ventricle, A+V) and atrioventricular canal (AVC) in (**a**). Data normalized to the mean fluorescence intensity of control hearts. (**c**) Representative confocal z-stack (maximal intensity projection) of control and *ift88* morpholino-injected *id2b:eGFP* embryos. (**d**) Normalized MFI of *id2b:eGFP* in the working myocardium (A+V) and AVC in (**c**). (**e**) Whole-mount *in situ* hybridization showing *id2b* expression in control, *klf2a*$^{-/-}$, and *klf2b*$^{-/-}$ embryos at 48 hpf and 72 hpf. Numbers at the bottom of each panel indicate the ratio of representative staining. Data are presented as mean ± sem. ** $p<0.01$, *** $p<0.001$, **** $p<0.0001$. Scale bars: 50 μm.

Figure 4. *id2b*$^{-/-}$ adults exhibit thinner atrioventricular valve leaflets and prominent retrograde blood flow.

(**a**) Two sgRNAs, represented by short vertical lines, were designed to create *id2b*$^{-/-}$ mutants. Co-injection of the two sgRNAs with zCas9 protein induces a 157 bp truncation in the exon 1 of *id2b*, which can be detected by genotyping primers marked with arrows. This genetic modification leads to the formation of a premature stop codon and the subsequent loss of the HLH domain. (**b**) No discernible morphological differences were observed between *id2b*$^{+/+}$ and *id2b*$^{-/-}$ larvae at both 72 hpf and 96 hpf. (**c**) Kaplan-Meier survival curve analysis and logrank test of *id2b*$^{+/+}$ (n=50) and *id2b*$^{-/-}$ (n=46). Wpf: weeks post-fertilization. (**d**) Pericardial edema and an enlarged atrium are evident in a

subset of *id2b*$^{-/-}$ adults. V, ventricle; A, atrium. (**e**) *id2b*$^{-/-}$ adults developed thinner atrioventricular valve leaflets (denoted by arrowheads) compared to *id2b*$^{+/+}$. Enlarged views of boxed areas are shown in the right panels. (**f**, **g**) Echocardiograms of adult *id2b*$^{+/+}$ (**f**) and *id2b*$^{-/-}$ (**g**) hearts. Unidirectional blood flow was observed in the *id2b*$^{+/+}$ heart, while retrograde blood flow was evident in the *id2b*$^{-/-}$ heart. (**h**) Ratio of retrograde flow area over inflow area shows a significant increase in retrograde flow in *id2b*$^{-/-}$ (n=13) compared to *id2b*$^{+/+}$ (n=10). Data are presented as mean ± sem. ** $p<0.01$. Scale bars: 200 μm (**e**); 500 μm (**b** and **d**, bottom); 2 mm (**d**, top).

Figure 5. Reduced cardiac contractile function and compromised calcium handling in *id2b*$^{-/-}$ mutants.

(**a**) Time-lapse imaging (from T1 to T8) illustrates the cardiac contraction-relaxation cycle of 120 hpf *id2b*$^{+/+}$ and *id2b*$^{-/-}$ hearts carrying *myl7:mCherry*. (**b** and **c**) *id2b*$^{-/-}$ larvae display a significant decrease in heart rate and fractional area change compared to *id2b*$^{+/+}$. (**d**) Echocardiograms of adult *id2b*$^{+/+}$ and *id2b*$^{-/-}$ hearts. (**e** and **f**) *id2b*$^{-/-}$ fish exhibit reduced cardiac contractile function with preserved heart rate compared to *id2b*$^{+/+}$. (**g**) Time-lapse imaging illustrates the calcium dynamics of 120 hpf *id2b*$^{+/+}$ and *id2b*$^{-/-}$ hearts carrying *actb2:GCaMP6s*. (**h**) Ratio of maximal fluorescence intensity (**F**) over basal fluorescence intensity (F0) of GCaMP6s signal. (**i**) qRT-PCR analysis of *cacnα1c* mRNA in *id2b*$^{+/+}$ and *id2b*$^{-/-}$ hearts at 120 hpf (N=three replicates, with each sample containing 500-1,000 embryonic hearts) and adult stage (N=five replicates). Data were normalized to the expression of *actb1*. (**j**) The action potential of ventricular cardiomyocyte in adult *id2b*$^{+/+}$ and *id2b*$^{-/-}$ hearts. (**k**) Statistical data showed a notable difference between *id2b*$^{+/+}$ and *id2b*$^{-/-}$ accordingly. Data are presented as mean ± sem. *** $p<0.001$, **** $p<0.0001$, ns, not significant. Scale bar: 50 μm.

Figure 6. *nrg1* serves as a pivotal mitogen mediating the function of *id2b*.

(**a**) Identification of genes (*fgf8a*, *nkx2.5*, *myh6*, *nrg1*, and *nkx2.7*) associated with four distinct heart development processes: cardiac muscle tissue development, cardiomyocyte differentiation, heart morphogenesis, and cardiac chamber development. The heatmap illustrates scaled-normalized expression values for the mentioned genes. (**b**) qRT-PCR analysis of *nrg1* mRNA in 120 hpf *id2b*$^{+/+}$

and *id2b*$^{-/-}$ embryonic hearts. Data were normalized to the expression of *actb1*. N=four replicates, with each sample containing 500-1,000 embryonic hearts. (**c**) *id2b*$^{+/+}$ and *id2b*$^{-/-}$ larvae were injected with *nrg1* mRNA at the 1-cell stage, followed by qRT-PCR analysis of *cacnα1c* mRNA at 72 hpf. Data were normalized to the expression of *actb1*. N=three replicates, with each samples containing 100-200 embryonic hearts. (**d**) The heart rate of 72 hpf *id2b*$^{+/+}$ and *id2b*$^{-/-}$ larvae injected with *nrg1* mRNA at 1-cell stage. (**e**) Heart rate in 120 hpf larvae treated with AG1478 and DMSO. Data are presented as mean ± sem. ∗ $p<0.05$, ∗∗ $p<0.01$, ∗∗∗ $p<0.001$, ∗∗∗∗ $p<0.0001$. ns, not significant.

Figure 7. *id2b* interacts with *tcf3b* to restrict its inhibition on *nrg1* expression.

(**a**) Immunoprecipitation (IP) assays of FLAG-*id2b* and HA-*tcf3b* co-transfected 293T cells. (**b**) qRT-PCR analysis of *tcf3a*, *tcf3b*, *socs1a*, and *socs3b* mRNA in 120 hpf *id2b*$^{+/+}$ and *id2b*$^{-/-}$ embryonic hearts. Data were normalized to the expression of *actb1*. N=three replicates, with each samples containing 500-1,000 embryonic hearts. (**c**) Two potential *tcf3*b binding sites, with sequences corresponding to the human tcf3 (left) and mouse tcf3 (right) binding motifs, were predicted in the 2,000bp DNA sequence upstream of the zebrafish *nrg1* transcription start site using JASPAR. (**d**) Luciferase assay showing the expression of *nrg1* in embryos with *tcf3b* overexpression (*tcf3b* OE) and morpholino-mediated *tcf3b* knockdown (*tcf3b* MO). N=three replicates. (**e**) qRT-PCR analysis of *nrg1* mRNA in 72 hpf *id2b*$^{+/+}$ and *id2b*$^{-/-}$ embryonic hearts injected with control and *tcf3b* morpholino. Data were normalized to the expression of *actb1*. N=three replicates, with each samples containing 100-200 embryonic hearts. (**f**) Schematic model for *id2b*-mediated regulation of myocardium function. During heart development, blood flow operates through primary cilia, initiating endocardial *id2b* expression. Subsequently, the interaction between *id2b* and *tcf3b* restricts the activity of *tcf3b*, ensuring proper *nrg1* expression, which in turn promotes LTCC expression (left). However, in the absence of *id2b*, *tcf3b* directly bind to the *nrg1* promotor, inhibiting its expression. The reduced *nrg1* hinders LTCC expression in cardiomyocytes, resulting in decreased extracellular calcium entry and disruption of myocardial function. Data are presented as mean ± sem. ∗ $p<0.05$, ∗∗ $p<0.01$, ∗∗∗ $p<0.001$, ∗∗∗∗ $p<0.0001$. ns, not significant.

Supplementary Figure S1. Blood flow and BMP signaling independently activates *id2b* expression.

(**a**) Representative confocal maximal intensity projection of control (non-injected), *bmp2b*, *bmp4*, and *bmp7a* morpholino-injected *id2b:eGFP*; *Tg*(*myl7:mCherry*) hearts at 72 hpf. (**b**) Quantification of mean fluorescence intensity of *id2b:eGFP* in (**a**). Data normalized to the mean fluorescence intensity of control hearts. (**c**) Representative confocal maximal intensity projection of DMSO and Dorsomorphin (DM)-treated *id2b:eGFP* hearts at 48 and 60 hpf. Embryos were treated from 24 to 48 hpf, or from 36 to 60 hpf. (**d**) Quantification of mean fluorescence intensity of *id2b:eGFP* in (**c**). Data normalized to the mean fluorescence intensity of DMSO-treated hearts. (**e**) Confocal optical sections of control, tricaine-treated, and *tnnt2a* morpholino-injected 72 hpf *Tg*(*Bre:d2GFP*); *Tg*(*myl7:mCherry*) hearts. Yellow arrowheads: endocardial cells. Numbers at the top of each panel indicate the ratio of representative images. (**f**) Schematic diagram of blood flow and BMP signaling-mediated *id2b* expression. Data are presented as mean ± sem. *** $p<0.001$, **** $p<0.0001$. ns, not significant.

Supplementary Figure S2. *id2b*$^{-/-}$ larvae exhibit a decreased number of valve endocardial cells while maintaining normal atrioventricular valve function.

(**a**) Representative confocal images of valve endocardial cells in 96 hpf *id2b*$^{+/+}$ and *id2b*$^{-/-}$ hearts carrying *Tg*(*kdrl:nucGFP)*. (**b**) Quantification of the number of valve endocardial cells in *id2b*$^{+/+}$ and *id2b*$^{-/-}$ hearts. VECs: valve endocardial cells. (**c**) Representative confocal images of 72 and 120 hpf *id2b*$^{+/+}$ and *id2b*$^{-/-}$ hearts in *Tg*(*kdrl:nucGFP*); *Tg*(*myl7:mCherry*) transgenic background. (**d**) Statistical analysis of the number of endocardial cells in the ventricle (V), atrium (A), and combined (A+V) in *id2b*$^{+/+}$ and *id2b*$^{-/-}$ hearts. (**e**) Quantification of blood flow patterns in 96 hpf *id2b*$^{+/+}$ and *id2b*$^{-/-}$ hearts. Data are presented as mean ± sem. **** $p<0.0001$. ns, not significant. Scale bars: 20 μm (**a**); 50 μm (**b**).

Supplementary Figure S3. *id2b* loss-of-function impacts both valve formation and cardiac contraction.

(**a**) The top 20 predicted tissue expression patterns based on the differential expressed genes from *id2b*$^{+/+}$ and *id2b*$^{-/-}$ hearts at 120 hpf were displayed. (**b**) The top 20 predicted phenotypes related to the differential expressed genes from *id2b*$^{+/+}$ and *id2b*$^{-/-}$ hearts at 120 hpf were illustrated.

Supplementary Figure S4. *id2b*$^{-/-}$ hearts develop normal trabeculae and sarcomeres.

(**a**) Representative confocal z-stack of 72 and 120 hpf *id2b*$^{+/+}$ and *id2b*$^{-/-}$ hearts with *Tg*(*myl7:H2A-mCherry*) transgene. (**b**) Quantification of the number of cardiomyocytes in the ventricle (V), atrium (A), and combined (A+V) in (**a**). (**c**) Representative confocal images of 72 and 120 hpf *id2b*$^{+/+}$ and *id2b*$^{-/-}$ hearts carrying *Tg*(*myl7:H2A-mCherry*). (**d**) Confocal immunofluorescence images of α-actinin (green) in embryonic (72 hpf) and adult (115 dpf) hearts (left). Right: fluorescence intensity profiles for α-actinin. Data are presented as mean ± sem. ns, not significant. Scale bars: 50 μm (**a** and **c**); 5 μm (**d**).

Supplementary Figure S5. *nrg1* is expressed in the endocardial cells.

(**a**) Analysis of *nrg1* expression using the zebrafish single-cell landscape database. The red rectangle highlights endocardial cells. (**b**) Identification of the endocardial cell population in the zebrafish cell landscape. Purple dots represent endocardial cells, and the red oval denotes cell populations from the heart. Images were generated using the Zebrafish Cell Landscape (ZCL) at http://bis.zju.edu.cn/ZCL/.

Supplementary Figure S6. Expression landscape of zebrafish *tcf3b*.

The major cell types expressing *tcf3b* were displayed according to the zebrafish single-cell landscape. Images were generated using the Zebrafish Cell Landscape (ZCL) at http://bis.zju.edu.cn/ZCL/.

Video 1. 96 hpf *id2b*$^{+/+}$ larvae displayed unidirectional blood flow in the AV canal. Scale bar: 50 μm.

Video 2. 96 hpf *id2b*$^{-/-}$ larvae displayed unidirectional blood flow in the AV canal. Scale bar: 50 μm.

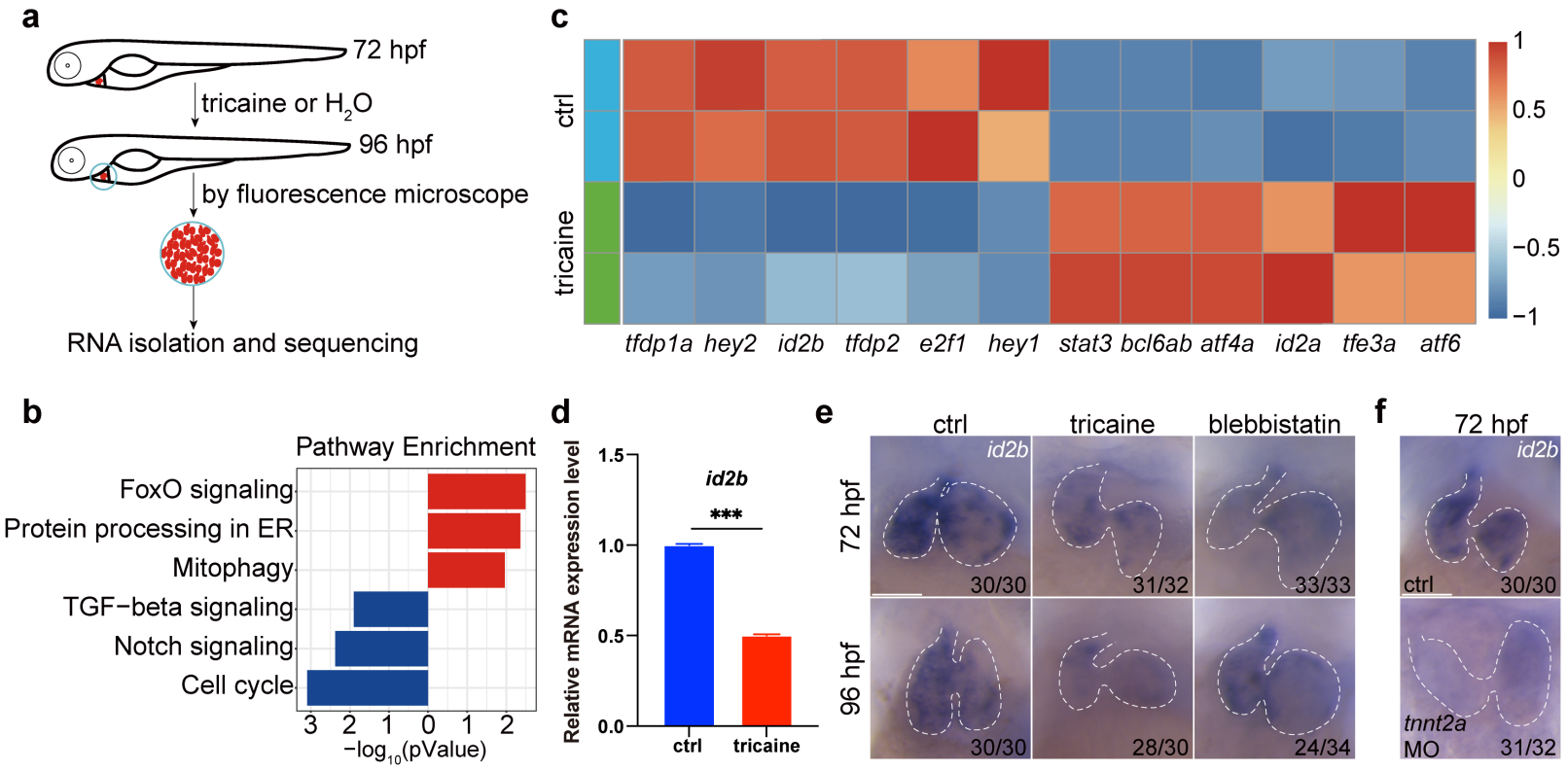
a
72 hpf
tricaine or H_2O
96 hpf
by fluorescence microscope
RNA isolation and sequencing
c
ctrl
tricaine
tfdp1a hey2 id2b tfdp2 e2f1 hey1 stat3 bcl6ab atf4a id2a tfe3a atf6
1
0.5
0
−0.5
−1
b
Pathway Enrichment
FoxO signaling
Protein processing in ER
Mitophagy
TGF−beta signaling
Notch signaling
Cell cycle
3 2 1 0 1 2
$-\log_{10}$(pValue)
d
Relative mRNA expression level
1.5
1.0
0.5
0.0
id2b
***
ctrl
tricaine
e
ctrl
tricaine
blebbistatin
72 hpf
96 hpf
id2b
30/30
31/32
33/33
30/30
28/30
24/34
f
72 hpf
id2b
ctrl
30/30
tnnt2a
MO
31/32

Figure 1

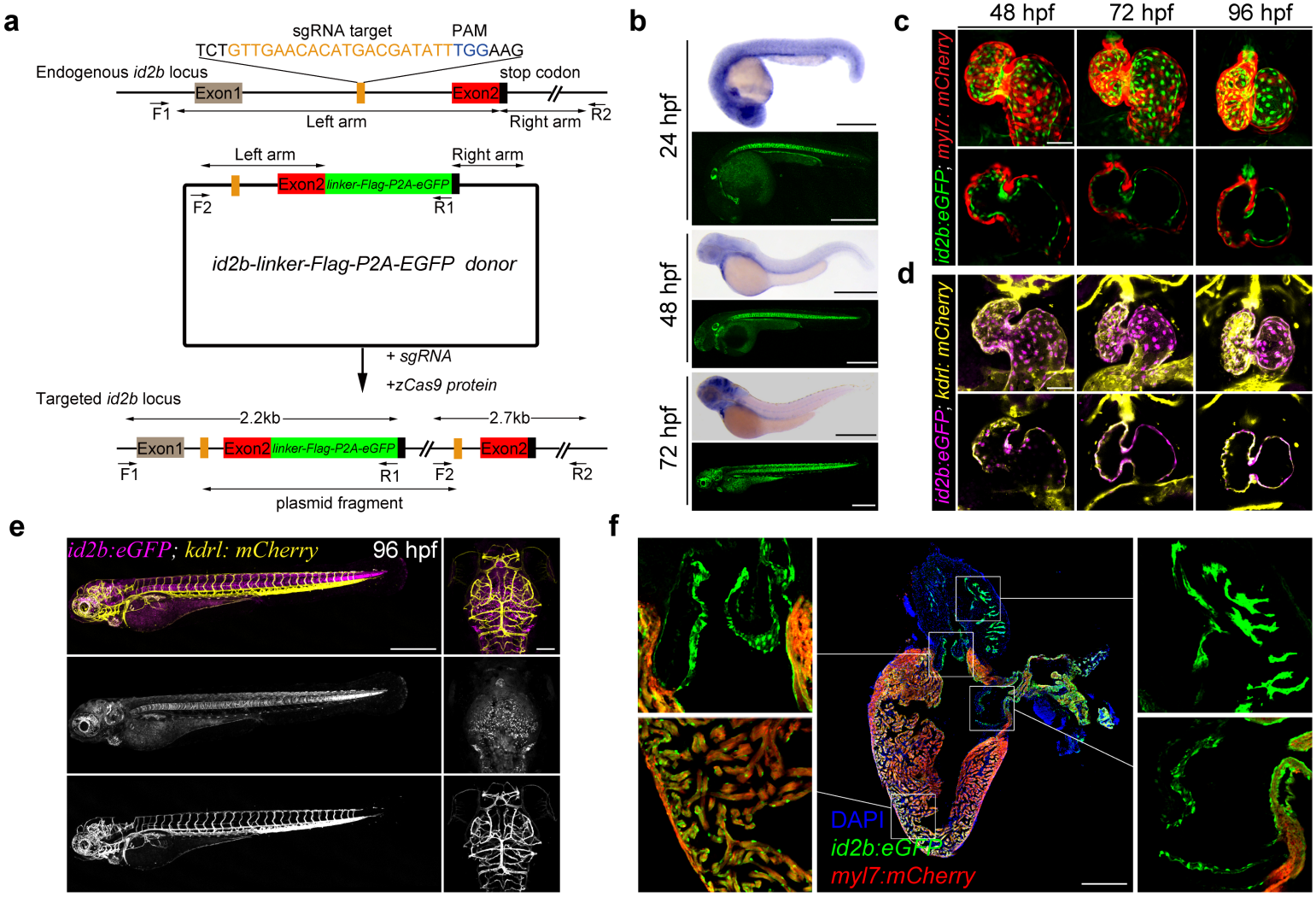
a
sgRNA target
PAM
TCTGTTGAACACATGACGATATTTGGAAG
Endogenous id2b locus
stop codon
Exon1
Exon2
F1
Left arm
Right arm
R2
Left arm
Right arm
Exon2
linker-Flag-P2A-eGFP
F2
R1
id2b-linker-Flag-P2A-EGFP donor
+ sgRNA
+zCas9 protein
Targeted id2b locus
2.2kb
2.7kb
Exon1
Exon2
linker-Flag-P2A-eGFP
Exon2
F1
R1
F2
R2
plasmid fragment
b
24 hpf
48 hpf
72 hpf
c
48 hpf
72 hpf
96 hpf
id2b:eGFP; myl7: mCherry
d
id2b:eGFP; kdrl: mCherry
e
id2b:eGFP; kdrl: mCherry
96 hpf
f
DAPI
id2b:eGFP
myl7:mCherry

Figure 2

Chen *et al.*

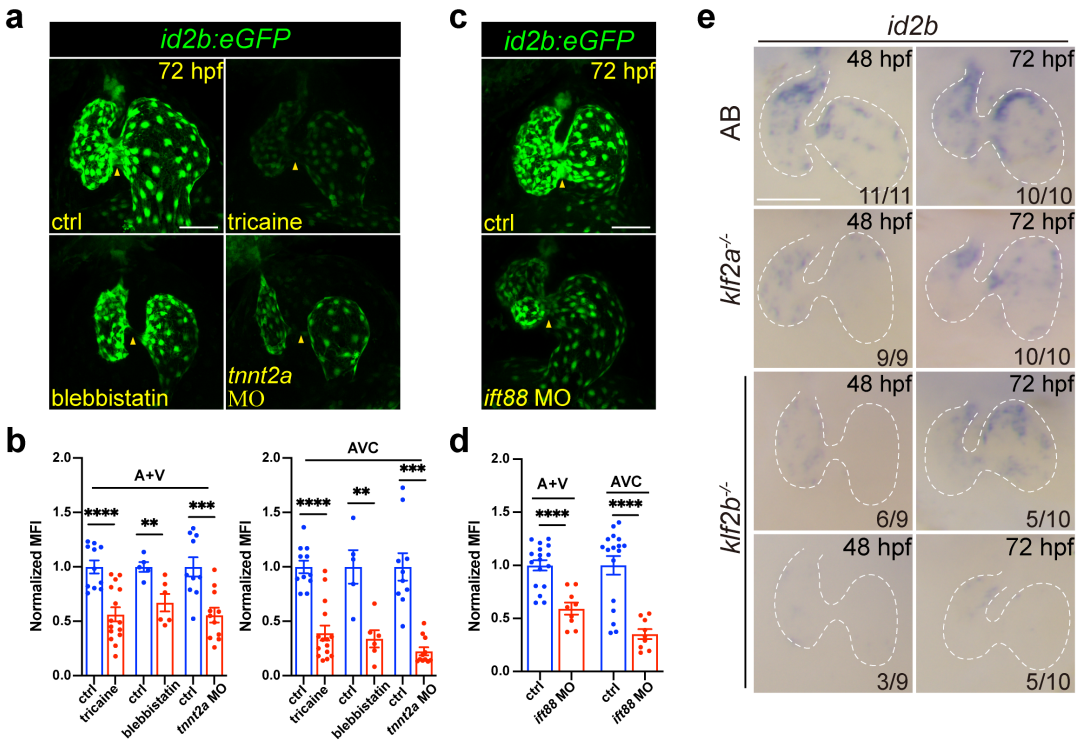

Figure 3

Chen *et al.*

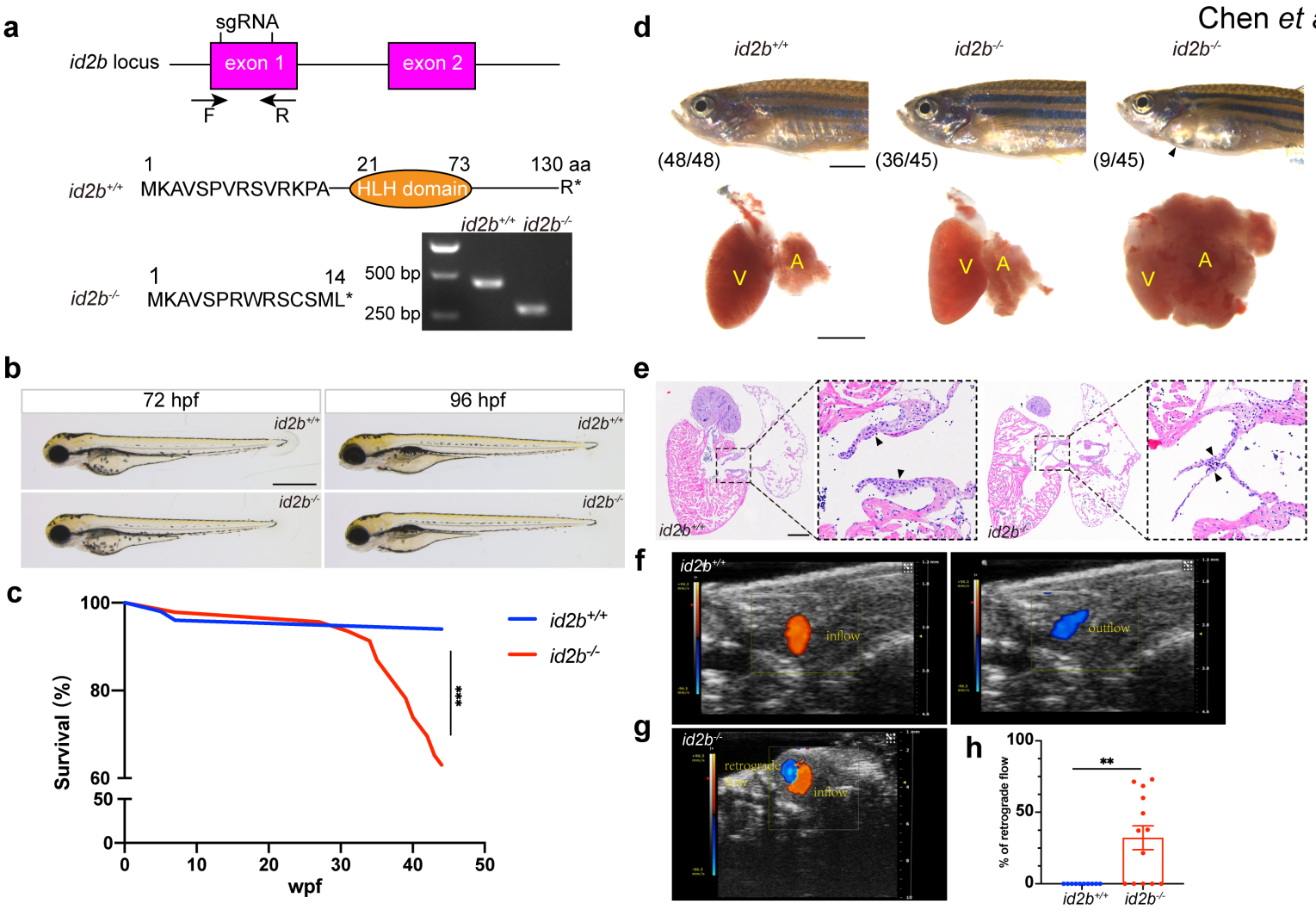

Figure 4

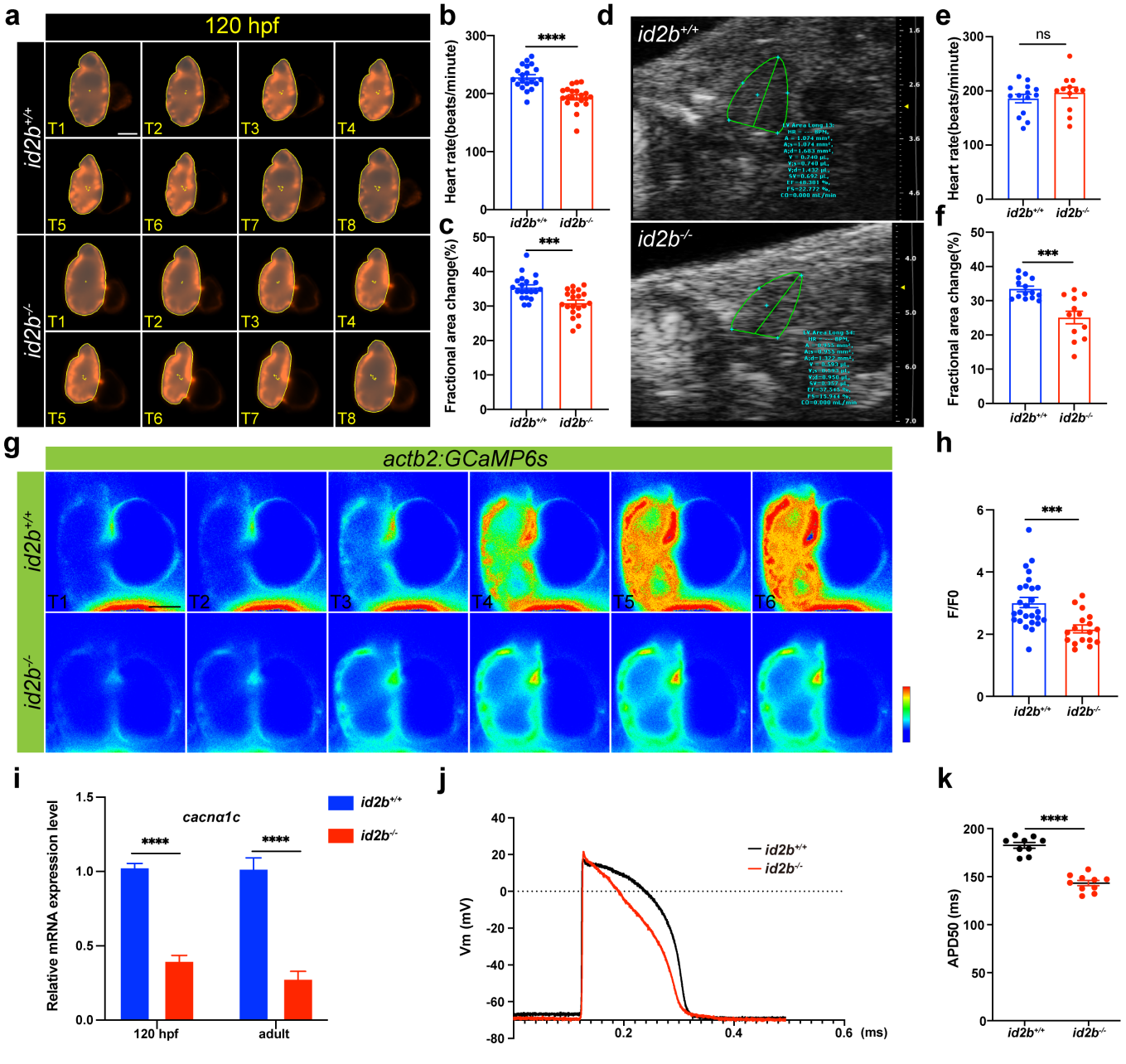
a
120 hpf
id2b+/+
id2b-/-
T1
T2
T3
T4
T5
T6
T7
T8
b
Heart rate(beats/minute)
****
id2b+/+
id2b-/-
c
Fractional area change(%)
***
d
id2b+/+
id2b-/-
e
Heart rate(beats/minute)
ns
f
Fractional area change(%)
***
g
actb2:GCaMP6s
h
F/F0
***
i
cacna1c
Relative mRNA expression level
****
120 hpf
adult
j
Vm (mV)
(ms)
k
APD50 (ms)
****

Figure 5

Chen *et al.*

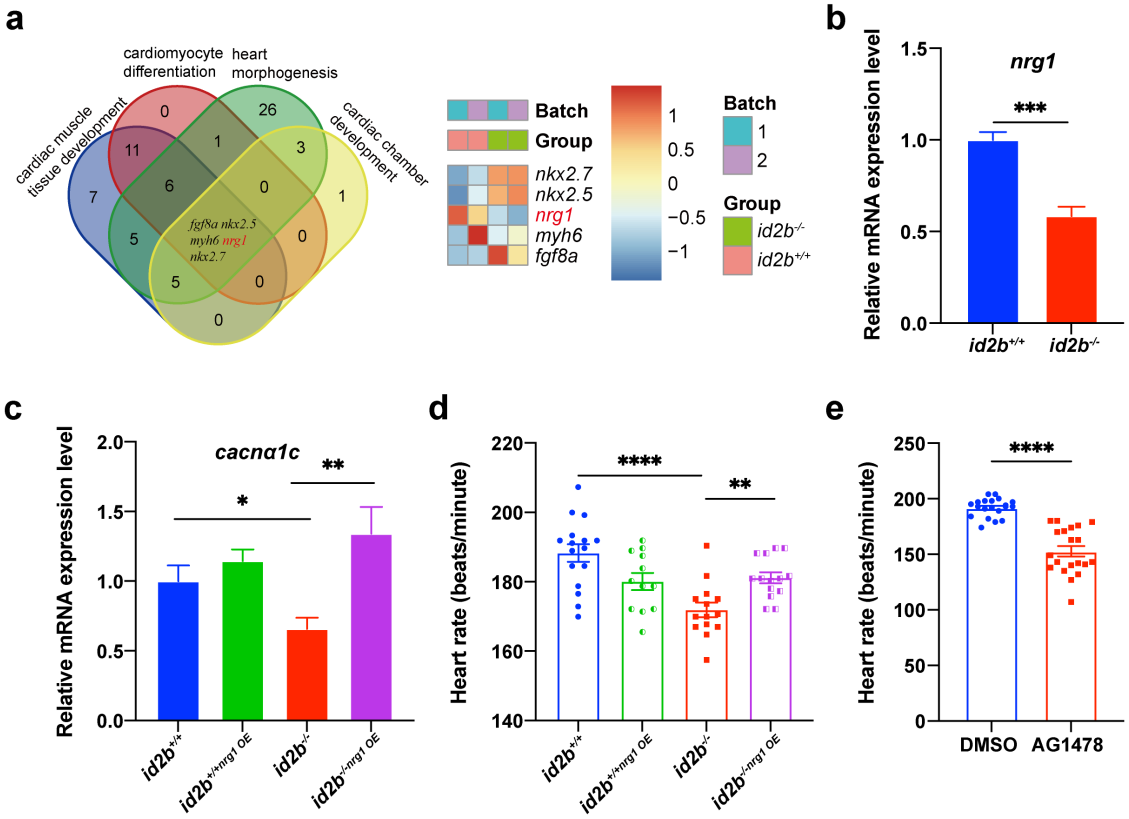

Figure 6

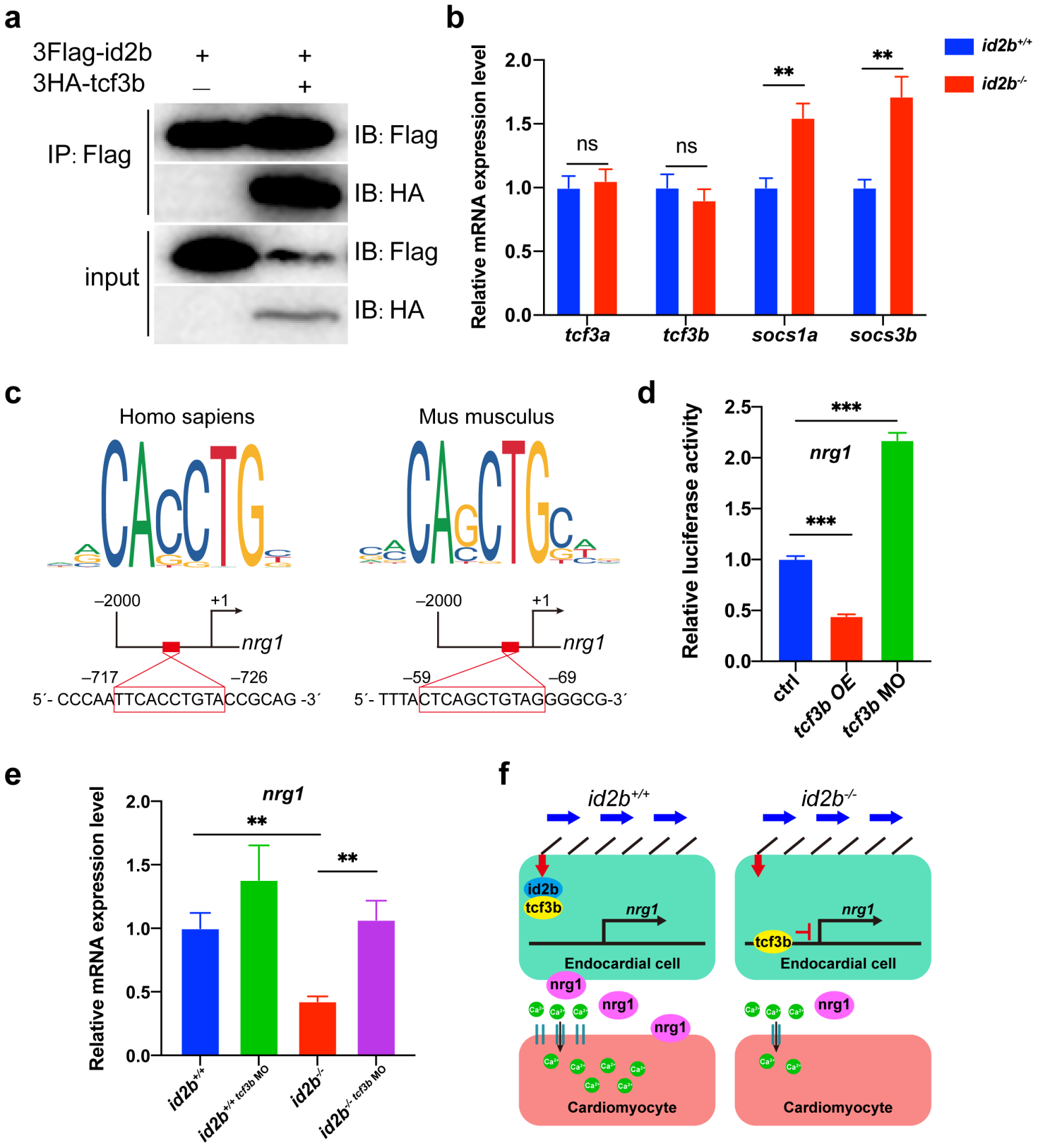
a
3Flag-id2b + +
3HA-tcf3b — +
IP: Flag
IB: Flag
IB: HA
input
IB: Flag
IB: HA
b
Relative mRNA expression level
2.0
1.5
1.0
0.5
0.0
ns
ns
**
**
tcf3a
tcf3b
socs1a
socs3b
id2b+/+
id2b-/-
c
Homo sapiens
Mus musculus
–2000
+1
nrg1
–717
–726
5´- CCCAATTCACCTGTACCGCAG -3´
–59
–69
5´- TTTACTCAGCTGTAGGGGCG-3´
d
Relative luciferase activity
2.5
2.0
1.5
1.0
0.5
0.0
***
***
nrg1
ctrl
tcf3b OE
tcf3b MO
e
Relative mRNA expression level
nrg1
2.0
1.5
1.0
0.5
0.0
**
**
id2b+/+
id2b+/+ tcf3b MO
id2b-/-
id2b-/- tcf3b MO
f
id2b+/+
id2b-/-
id2b
tcf3b
nrg1
Endocardial cell
tcf3b
nrg1
Endocardial cell
nrg1
nrg1
nrg1
nrg1
Cardiomyocyte
Cardiomyocyte

Figure 7